THE UNIVERSITY OF READING

EVALUATION OF THE PROPOSED NEW UNIFIED MODEL SCHEME vs THE CURRENT UNIFIED MODEL SCHEME ON THE SHALLOW WATER EQUATIONS

by

A.J. Malcolm

Numerical Analysis Report 1/96

DEPARTMENT OF MATHEMATICS

Evaluation of the Proposed New Unified Model Scheme vs the Current Unified Model Scheme on the Shallow Water Equations. [1]

A.J. Malcolm

Final Report

Department of Mathematics

P.O.Box 220

University of Reading

Whiteknights

Reading

RG6 6AF

United Kingdom

[1]The work reported here forms part of the research programme of the Oxford/Reading Institute for Computational Fluid Dynamics and was supported by the Met. Office, Bracknell under contract MET 2a/0471.

Abstract

All predictive models used in numerical weather prediction involve the treatment of advective terms. The "unified model" which is employed by the Met Office for numerical weather prediction includes such terms. It has never been fully tested and, with a proposal to totally revise the "unified model" including a change of the model's numerical scheme from split-explicit Eulerian to semi-implicit semi-Lagrangian, a number of tests are implemented on the possible revisions of the "unified model". One such test is that both the current and the proposed new numerical schemes should be tested against each other and other alternative schemes.

The numerical schemes are tested on the Shallow Water Equations on a suite of standard test problems. Numerical and graphical results are produced to allow a comprehensive comparison of the schemes.

Conclusions are drawn as to whether the current Eulerian scheme is the better of the two and to whether the proposed new scheme will result in an improvement to the numerical solution for the "unified model".

Contents

1 Introduction

All predictive models used in numerical weather prediction involve the treatment of advective terms. The "unified model" which is employed by the Met Office for numerical weather prediction includes such terms [3], [4].

Present day numerical weather prediction (NWP) involves solving a form of the Navier-Stokes equations for a fluid on a rotating sphere together with conservation of mass (continuity equation), an energy equation and a transport equation for water vapour.

The Eulerian equations of motion contain the familiar, non-linear advection terms and adjustment terms involving large-scale balance between pressure gradient and coriolis forces.

In major forecast centres such as the UK Meteorological Office, the numerical models have to be robust and reliable and are run routinely to tight schedules. This necessitates the use of efficient numerical methods. Similar models used for climate research also need to be efficient as simulations may be run for thousands of years. The numerical solvers used are generally not as advanced as those used in other areas of computational fluid dynamics although there is a growing use of, for example, semi-Lagrangian schemes and TVD or shape preserving advection schemes.

As part of a programme for improving the UK Meteorological office Unified model, which is used for operational (daily) NWP and climate research (general circulation models), the numerical schemes used have been tested on a standard set of test problems, [13] designed to show their performance in solving the solution of the Shallow Water Equations (SWE) on a sphere. The SWE are outlined in Section 2. The testing requires that the numerical schemes used for the unified model equations are tailored to the SWE. The SWE are discretised using finite differences on the Arakawa B-grid. The main numerical scheme tested is a split-explicit Eulerian conservative fourth order Heun advection scheme [2]. Lower order advection schemes were also tested as were, for the simplest test case, a TVD [8] and a semi-Lagrangian [1] scheme. All of the Eulerian schemes are described in Sections 3.1 to 3.4.

The proposed new scheme is then tailored to the SWE. The SWE are discretised on the Arakawa C-grid and a semi-implicit semi-Lagrangian scheme applied on the grid. This procedure is detailed in Section 3.5.

The suite of test problems ranges from pure advection, through steady state solutions to the SWE and problems with orography to the Rossby-Haurwitz problem and actual observed data.

These are detailed in Sections 4.1 to 4.7.

The results of all the procedures are compared, using the error measures detailed in Section 4.8, and conclusions are drawn as to the viability of the proposed new scheme. The results and conclusions are outlined in Section 5. The study of the results from the test suite has produced additional data with which to make a choice of diffusion coefficient for the current scheme.

2 Shallow Water Equations on a Sphere

Consider the SWE on the sphere, which are

$$\frac{\partial u}{\partial t} + \frac{u}{a\cos\phi}\frac{\partial u}{\partial \lambda} + \frac{v}{a}\frac{\partial u}{\partial \phi} - \left(f + \frac{u}{a}\tan\phi\right)v + \frac{g}{a\cos\phi}\frac{\partial h}{\partial \lambda} = 0, \tag{1}$$

$$\frac{\partial v}{\partial t} + \frac{u}{a\cos\phi}\frac{\partial v}{\partial \lambda} + \frac{v}{a}\frac{\partial v}{\partial \phi} + \left(f + \frac{u}{a}\tan\phi\right)u + \frac{g}{a}\frac{\partial h}{\partial \phi} = 0, \tag{2}$$

together with the continuity equation

$$\frac{\partial h^*}{\partial t} + \nabla.(h^*\boldsymbol{u}) = 0, \tag{3}$$

where h is the height, h_s is the height of any orography with $h^* = h - h_s$, (λ, ϕ) are the spherical coordinates, (u, v) are the velocities in the λ and ϕ coordinate directions respectively with $\boldsymbol{u} = (u, v)^T$, g is gravity and a is the radius of the earth.

2.1 Differences between the "unified model" and the Shallow Water Equations

The major differences between these equations and those in the unified model [3], [4] are that there is no vertical velocity and there is only one h level in the vertical, which means that, as far as the unified model is concerned, the k subscripts in the documentation can be ignored. The quantities θ, virtual potential temperature, and Φ, topographic height, do not arise in the SWE. For clarity the i, j subscripts are suppressed. Any physics and chemistry is ignored.

2.2 "Eulerian" and "semi-Lagrangian" methods

Numerical solutions of equations do not give a continuous solution for any variable, but rather they give values for a variable at a discrete set of grid points. Eulerian schemes depend only on

the data values at these discrete points and so the information needed for a numerical solution is passed forward from grid point to grid point.

This is different from a semi-Lagrangian scheme where, in order to calculate grid point values, you calculate where a parcel of fluid would start from to end up at the grid point. (This departure point is not necessarily a grid point). The value of the variable at the departure point is then used as the value of the variable at the grid point where it arrives for the next time level. Since the data values are only held at grid points, to find the data value at the departure point requires the use of an interpolation procedure. This procedure finds which grid cell the departure point is in and then using neighbouring grid point values produces a value at the departure point. The simplest interpolation is bi-linear, which only requires the data values at the corners of the enclosing grid box. Other more expensive, but more accurate, choices are cubic and quintic interpolation.

2.3 Grids and Notation

The computational grid used for the Eulerian scheme is an Arakawa 'B' grid (see Figure 1). The grid axes are in the λ and ϕ directions. The grid is N_λ by N_ϕ points, giving grid spacings of $\Delta\lambda = 2\pi/N_\lambda$ and $\Delta\phi = \pi/(N_\phi - 1)$ where $\lambda \in [0, 2\pi]$ and $\phi \in [-\pi/2, \pi/2]$, with $\phi = 0$ the equator, $\phi = \pi/2$ the North Pole and $\phi = -\pi/2$ the South Pole. This means that the North Pole is actually represented by a line of N_λ points, i.e. the grid line $j = 1$. The Arakawa B grid holds the values of the height field at each grid point with the velocity field being held at the centre of each grid cell. The height field is therefore of array dimension N_λ by N_ϕ, whilst both the velocity components are fields of array dimension N_λ by $N_\phi - 1$. The grid size used for most of the results in this paper is 96x73. However some more practical simulations are run on grids up to a size of 288x217 points.

The semi-Lagrangian scheme is run on an Arakawa C-grid. With this grid the variables are held at different points than on a B-grid (see Figure 1). The grid spacings are calculated as for a B-grid. However for the semi-Lagrangian scheme the point ordering has changed and the North Pole is now represented by a line of N_λ points, i.e. the grid line $j = N_\phi$. The Arakawa C-grid holds the values of the height field at each grid point with the u component of the velocity held on a horizontal grid box side and the v component of the velocity held on a vertical grid box side. The height field, and the u field, are therefore arrays of dimension N_λ by N_ϕ, whilst the v

field is an array of dimension N_λ by $N_\phi - 1$. The grid size used for most of the results in this paper is 96x65.

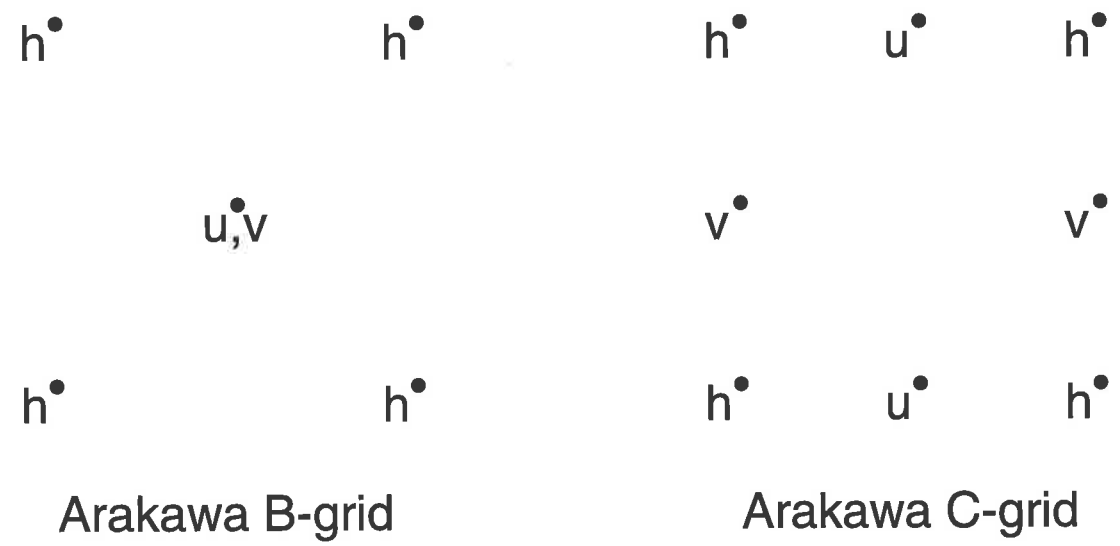

Figure 1: Distribution of grid points.

In the discretisations that follow the notation used for differences and averages is:-

$$\delta_\lambda X = \frac{[X(\lambda + \frac{1}{2}\Delta\lambda) - X(\lambda - \frac{1}{2}\Delta\lambda)]}{\Delta\lambda},$$

$$\overline{X}^{\lambda} = \frac{1}{2}[X(\lambda + \frac{1}{2}\Delta\lambda) + X(\lambda - \frac{1}{2}\Delta\lambda)],$$

$$\overline{X}^{3\lambda} = \frac{1}{2}[X(\lambda + \frac{3}{2}\Delta\lambda) + X(\lambda - \frac{3}{2}\Delta\lambda)],$$

$$\overline{X}^{\lambda\phi} = \overline{\overline{X}^{\lambda}}^{\phi}.$$

The notation X_d means that the variable X is evaluated at the departure point d (see Section 2.2) using interpolation.

3 Numerical schemes

In this section the numerical schemes which were tested are presented. The Eulerian schemes are presented first, followed by the semi-Lagrangian scheme. The first Eulerian scheme presented is the fourth-order Heun scheme presently used in the "unified model". This is then followed by a

simplified Heun scheme and a Lax-Wendroff scheme. A TVD scheme is then outlined and finally the semi-Lagrangian solution procedure is detailed.

For a description of the code logic over one time step, the problems with the initial documentation for the current scheme and the problems encountered with all the Eulerian schemes, see [10].

3.1 The Heun scheme

The split-explicit Eulerian scheme in [3] seeks to combine accuracy and efficiency and preserve the conservation properties required for long-term climate integrations. A Heun scheme, with Euler time stepping, is used for the advection which allows for 2nd or 4th order accuracy in space. Various quantities are conserved under the Eulerian schemes outlined.

Rather than treat the complete set of equations in one step, they are split into two separate parts. This is due to the fact that certain of the terms in the equations can be treated on different time scales from the others. Those terms whose numerical treatments require a small time step, due to the CFL condition, are solved more often than those which can use a large time step.

Before discretisation, equations (1) and (2) are split into an adjustment step and an advection step. The advection step solves $\frac{\partial \boldsymbol{u}}{\partial t}+\boldsymbol{u}.\nabla \boldsymbol{u} = 0$ while the adjustment step solves for the remaining terms in equations (1) and (2). The adjustment step requires a smaller time step so is carried out a number of times for every advection step taken.

The elements of the discretised forms of equations (1) and (2) which form the adjustment step are manipulated to form a pair of coupled equations,

$$u^{n+1} = u^n + \delta t \left[\frac{1}{2}F_n(v^{n+1} + v^n) - \frac{g}{a\cos\phi}\overline{\delta_\lambda h^n}^{\phi}\right], \tag{4}$$

$$v^{n+1} = v^n - \delta t \left[\frac{1}{2}F_n(u^{n+1} + u^n) + \frac{g}{a}\overline{\delta_\phi h^n}^{\lambda}\right], \tag{5}$$

where

$$F_n = f + \frac{u^n}{a}tan\phi \qquad \text{and} \qquad f = 2\Omega\sin\phi_A. \tag{6}$$

Eliminating u^{n+1} from equations (4) and (5) gives

$$v^{n+1} = \frac{v^n\left[1 - \frac{\delta t^2}{4}F_n^2\right] - \frac{\delta t}{2}\left\{2F_n u^n + \frac{2g}{a}\overline{\delta_\phi h^n}^{\lambda} - \frac{g\delta t}{a\cos\phi}\overline{\delta_\lambda h^n}^{\phi}F_n\right\}}{\left(1 + \frac{\delta t^2}{4}F_n^2\right)}$$

while eliminating v^{n+1} from equations (4) and (5) gives a corresponding expression for u^{n+1}.

Before the remaining terms in equations (1) and (2) can be employed in the advection step it is necessary to calculate a new height field, h^{n+1}, which can be found using the time stepping

$$h^{n+1} = h^n - \frac{\delta t}{a^2} D, \tag{7}$$

where

$$D = \frac{a}{\cos\phi}(\overline{\delta_\lambda(u\overline{h}^{\lambda\phi})}^{\phi} + \overline{\delta_\phi(v\overline{h}^{\lambda\phi}\cos\phi)}^{\lambda}) \tag{8}$$

gives a numerical approximation to $\nabla.(h\boldsymbol{u})$.

The treatment of the terms in equations (1) and (2) other than $-\boldsymbol{u}.\nabla\boldsymbol{u}$ can now be implemented during the advection step. In the advection step a new vector $\boldsymbol{U}$ is defined which is an averaged height weighted velocity field, namely

$$\boldsymbol{U} = (U, V) = \frac{\sum_{i=1}^{N_A}(au_i\overline{h_i}^{\lambda\phi}, av_i\cos\phi\overline{h_i}^{\lambda\phi})}{N_A}, \tag{9}$$

where N_A is the number of adjustment steps.

The fourth order Heun scheme, as implemented in [2], is then used to produce new values $u^\#$ and $v^\#$ for u and v from the equations

$$\begin{aligned} a^2\overline{h^n}^{\lambda\phi}u^\# &= a^2\overline{h^n}^{\lambda\phi}u^n - \\ &\frac{\Delta t}{\cos\phi}\left((1+\nu)\overline{\overline{U}^{\lambda\phi}\delta_\lambda u}^{\lambda} + (1+\nu)\overline{\overline{V}^{\lambda\phi}\delta_\phi u}^{\phi} - \nu\overline{\overline{U}^{\lambda\phi}\delta_\lambda u}^{3\lambda} - \nu\overline{\overline{V}^{\lambda\phi}\delta_\phi u}^{3\phi}\right) \end{aligned} \tag{10}$$

$$\begin{aligned} a^2\overline{h^n}^{\lambda\phi}v^\# &= a^2\overline{h^n}^{\lambda\phi}v^n - \\ &\frac{\Delta t}{\cos\phi}\left((1+\nu)\overline{\overline{U}^{\lambda\phi}\delta_\lambda v}^{\lambda} + (1+\nu)\overline{\overline{V}^{\lambda\phi}\delta_\phi v}^{\phi} - \nu\overline{\overline{U}^{\lambda\phi}\delta_\lambda v}^{3\lambda} - \nu\overline{\overline{V}^{\lambda\phi}\delta_\phi v}^{3\phi}\right), \end{aligned} \tag{11}$$

$$a^2\overline{h^{n+1}}^{\lambda\phi}u^{n+1} = a^2\overline{h^{n+1}}^{\lambda\phi}u^n - \frac{\Delta t}{2}\left(\overline{\left(\frac{h^{n+1}}{h^n}\right)}^{\lambda\phi}\boldsymbol{U}.\nabla u^n + \boldsymbol{U}.\nabla u^\#\right) \tag{12}$$

$$a^2\overline{h^{n+1}}^{\lambda\phi}v^{n+1} = a^2\overline{h^{n+1}}^{\lambda\phi}v^n - \frac{\Delta t}{2}\left(\overline{\left(\frac{h^{n+1}}{h^n}\right)}^{\lambda\phi}\boldsymbol{U}.\nabla v^n + \boldsymbol{U}.\nabla v^\#\right), \tag{13}$$

where ν is defined as $\nu = \nu_b(1-\xi_{\max}^2)$. The choice $\nu_b = 0$ defines a 2nd order scheme and $\nu_b = \frac{1}{6}$ defines a 4th order scheme. The minimum value for ν is zero which gives 2nd order accurate space advection. The quantity $\xi_{\max}$ is defined as the maximum ξ along a line of latitude or longitude as appropriate, with ξ being defined by

$$\xi = (\frac{u^2\Delta t^2}{a^2\Delta\lambda^2\cos^2\phi} + \frac{v^2\Delta t^2}{a^2\Delta\phi^2})^{\frac{1}{2}}. \tag{14}$$

If required, diffusion of order $2j$ of any variable, X, may be added into the scheme using the additional term $(-1)^{j-1}D^jX$ where, for example, if $j = 3, D^3X = D(D(D(X)))$ and where $D(X)$ is defined by

$$D(X) = \frac{1}{a^2 h^{n+1}} \left(\frac{1}{\cos^2 \phi} \delta_\lambda (\overline{k_x(\lambda,\phi)}^{\phi} \delta_\lambda X) + \frac{1}{\cos \phi} \delta_\phi (\overline{k_y(\lambda,\phi)}^{\lambda} \cos\phi \delta_\phi X) \right) \tag{15}$$

with

$$k_y(\lambda,\phi) = h^{n+1}k \qquad\qquad k_x(\lambda,\phi) = k_y(\lambda,\phi) \left(\frac{\Delta\lambda \cos\phi}{\Delta\phi} \right)^2 \tag{16}$$

and k is a user chosen coefficient where for stability we require

$$\Delta t \left(\frac{4k}{a^2 \Delta\phi^2} \right)^j \leq 1.$$

These are the main procedures implemented in a time-step of the numerical algorithm tested here, but there are other procedures mentioned in [3]. The grid splitting mentioned in Section 3.2 of [3] is not implemented since the use of a 4th order advection scheme renders it redundant. Divergence damping is also not employed, but Fourier filtering is used to prevent the timestep being undesirably reduced by the short gridlengths used in high latitudes.

Fourier filtering is implemented to reduce the amplitude of unstable wavelengths in the numerical solution. The solution vector is decomposed into its component waves, each of which has a certain amplitude. If the timestep is such that the numerical solution is unstable at particular latitudes, then a criterion is used to determine which wavelengths are unstable, and once the relevant wavelengths are found their amplitude is decreased by reducing the corresponding coefficients, or even setting the amplitude to zero (Fourier chopping). The solution vector is then reconstructed using the modified amplitudes.

The fourth order Heun scheme given in equations (10) to (13) is used in the advection step, although in the results presented here we not only produce results from the Heun scheme (as given in [10]) but also those from a simplified version of the Heun scheme and from a Lax-Wendroff scheme as well (see below).

3.2 Simplified Heun scheme

The simplified Heun scheme requires a new notation for differences, namely

$$\delta_{2\lambda} X = \frac{[X(\lambda + \Delta\lambda) - X(\lambda - \Delta\lambda)]}{2\Delta\lambda}$$

together with $\boldsymbol{U} = (u, v)^T$.

The same solution procedure as in Section 3.1 is employed but equations (10)-(13) are then solved using the Heun scheme below.

$$u^{\#} = u^n - \frac{\Delta t}{a\cos\phi}\left(u^n \delta_{2\lambda} u^n + v^n \cos\phi \delta_{2\phi} u^n\right) \tag{17}$$

$$v^{\#} = v^n - \frac{\Delta t}{a\cos\phi}\left(u^n \delta_{2\lambda} v^n + v^n \cos\phi \delta_{2\phi} v^n\right), \tag{18}$$

$$u^{n+1} = u^n - \frac{\Delta t}{2a}\left(\boldsymbol{U}.\nabla u^n + \boldsymbol{U}.\nabla u^{\#}\right) \tag{19}$$

$$v^{n+1} = v^n - \frac{\Delta t}{2a}\left(\boldsymbol{U}.\nabla v^n + \boldsymbol{U}.\nabla v^{\#}\right). \tag{20}$$

In equations (19) and (20) the terms $\boldsymbol{U}.\nabla u^n$ and $\boldsymbol{U}.\nabla v^n$ are actually the terms inside the brackets in equations (17) and (18) respectively. The terms $\boldsymbol{U}.\nabla u^{\#}$ and $\boldsymbol{U}.\nabla v^{\#}$ are calculated exactly as in equations (17) and (18) but with u^n and v^n replaced by $u^{\#}$ and $v^{\#}$.

3.3 Lax-Wendroff scheme

The same solution procedure as in Section 3.1 is employed but equations (10)-(13) are then solved using the Lax-Wendroff scheme as detailed below.

The Lax Wendroff scheme is slightly different in that the velocity values, $(u^{\#}, v^{\#})$, are held on the h grid points. The scheme is:

$$u^{\#} = \overline{u^n}^{\lambda\phi} - \frac{\Delta t}{2a\cos\phi}\left(\overline{u^n}^{\lambda\phi}\overline{\delta_\lambda u}^{\phi} + \overline{v^n}^{\lambda\phi}\cos\phi\overline{\delta_\phi u}^{\lambda}\right) \tag{21}$$

$$v^{\#} = \overline{v^n}^{\lambda\phi} - \frac{\Delta t}{2a\cos\phi}\left(\overline{u^n}^{\lambda\phi}\overline{\delta_\lambda v}^{\phi} + \overline{v^n}^{\lambda\phi}\cos\phi\overline{\delta_\phi v}^{\lambda}\right), \tag{22}$$

$$u^{n+1} = u^n - \frac{\Delta t}{2a\cos\phi}\left(\overline{u^{\#}}^{\lambda\phi}\overline{\delta_\lambda u^{\#}}^{\phi} + \overline{v^{\#}}^{\lambda\phi}\cos\phi\overline{\delta_\phi u^{\#}}^{\lambda}\right) \tag{23}$$

$$v^{n+1} = v^n - \frac{\Delta t}{2a\cos\phi}\left(\overline{u^{\#}}^{\lambda\phi}\overline{\delta_\lambda v^{\#}}^{\phi} + \overline{v^{\#}}^{\lambda\phi}\cos\phi\overline{\delta_\phi v^{\#}}^{\lambda}\right). \tag{24}$$

3.4 TVD Scheme

Another method tested was a TVD scheme for the treatment of advection. This TVD scheme is the one documented in [8]. It was set up to use either a superbee or Van Leer limiter and both were tested.

This scheme was only used for the first test case (see Section 4.1) which tests the advection scheme only.

Only equation (3) is solved in this case, the velocity fields being set initially and then fixed and only the height field evolved.

The procedure is as follows:-

1. At point $(\lambda + \frac{\Delta\lambda}{2}, \phi)$ calculate $\frac{\overline{u}^{\phi}}{a\cos\phi}\delta_{\lambda}h$

2. If $\overline{u}^{\phi} \geq 0$, subtract B from h at (λ, ϕ) and $(\frac{\overline{u}^{\phi}\Delta t}{a\cos\phi}\delta_{\lambda}h - B)$ from h at $(\lambda + \Delta\lambda, \phi)$ where

$$\begin{aligned} B \;=\; B\Bigg[& \frac{\nu_{\lambda+\frac{\Delta\lambda}{2}}}{2} + \frac{\Delta\lambda}{2}(1 - |\nu|_{\lambda+\frac{\Delta\lambda}{2}})\frac{(h_{\lambda+\Delta\lambda} - h_{\lambda})}{a\cos\phi}, \\ & \frac{\nu_{\lambda-\frac{\Delta\lambda}{2}}}{2} + \frac{\Delta\lambda}{2}(1 - |\nu|_{\lambda-\frac{\Delta\lambda}{2}})\frac{(h_{\lambda} - h_{\lambda-\Delta\lambda})}{a\cos\phi}\Bigg]. \end{aligned} \tag{25}$$

If $\overline{u}^{\phi} < 0$, subtract B from h at $(\lambda + \Delta\lambda, \phi)$ and $(\frac{\overline{u}^{\phi}\Delta t}{a\cos\phi}\delta_{\lambda}h - B)$ from h at (λ, ϕ) where

$$\begin{aligned} B \;=\; B\Bigg[& \frac{\nu_{\lambda+\frac{\Delta\lambda}{2}}}{2} + \frac{\Delta\lambda}{2}(1 - |\nu|_{\lambda+\frac{\Delta\lambda}{2}})\frac{(h_{\lambda+\Delta\lambda} - h_{\lambda})}{a\cos\phi}, \\ & \frac{\nu_{\lambda+\frac{3\Delta\lambda}{2}}}{2} + \frac{\Delta\lambda}{2}(1 - |\nu|_{\lambda+\frac{3\Delta\lambda}{2}})\frac{(h_{\lambda+2\Delta\lambda} - h_{\lambda+\Delta\lambda})}{a\cos\phi}\Bigg] \end{aligned} \tag{26}$$

where $\nu = \overline{u}^{\phi}\frac{\Delta t}{\Delta\lambda}$ is calculated at the appropriate λ and

$$\begin{aligned} B(b_1, b_2) &= b_2\max(b_1/b_2, 1) && \text{if } \tfrac{1}{2} < b_1/b_2 < 2 \\ &= 0 && \text{if } b_1/b_2 \leq 0 \\ &= 2b_2\min(b_1/b_2, 1) && \text{otherwise} \end{aligned} \tag{27}$$

3. Perform similar calculations at $(\lambda, \phi + \frac{\Delta\phi}{2})$ using $\frac{\overline{v}^{\lambda}}{a}\delta_{\phi}h$.

The time step is split up, on each row, into a number of smaller steps which do not violate the CFL at any grid point on that row. This is necessary due to small grid lengths on rows near the pole causing a need for smaller time steps there than on rows near the equator.

3.5 The semi-implicit semi-Lagrangian scheme.

These equations are rewritten in the form of the equations in [4]. Following the notation of that working paper the shallow-water algorithm is written as follows.

The scheme is basically a predictor-corrector scheme. In the first step the wind field at the next time step is predicted and the increments from the current time step to the next are calculated and stored. The correction comes from the continuity equation and results in the formulation of a Helmholtz equation, with respect to the increment in the height field. Then the wind fields are corrected to give final values for all the variables.

The predictive increments to the wind field are calculated in two parts, S_1 and S_2, which are the increments due to the forcing terms in the dynamics and R_1 and R_2, which are the full increments.

The first estimates to these wind field increments are given by

$$R_1 = u_d^n + 2\Omega\Delta t([(1-\alpha_1)\overline{v}^{\lambda\phi}\sin\phi]_d + \alpha_1\overline{v}^{\lambda\phi}\sin\phi) - \frac{g\Delta t}{a}([(1-\alpha_3)\frac{\delta_\lambda h}{\cos\phi}]_d + \alpha_3\frac{\delta_\lambda h}{\cos\phi}) - u^n \quad (28)$$

with

$$S_1 = 2\Omega\Delta t([(1-\alpha_1)\overline{v}^{\lambda\phi}\sin\phi]_d + \alpha_1\overline{v}^{\lambda\phi}\sin\phi) - \frac{g\Delta t}{a}([(1-\alpha_3)\frac{\delta_\lambda h}{\cos\phi}]_d + \alpha_3\frac{\delta_\lambda h}{\cos\phi}), \quad (29)$$

$$R_2 = v_d^n - 2\Omega\Delta t([(1-\alpha_1)\overline{u}^{\lambda\phi}\sin\phi]_d + \alpha_1\overline{u}^{\lambda\phi}\sin\phi) - \frac{g\Delta t}{a}([(1-\alpha_3)\delta_\phi h]_d + \alpha_3\delta_\phi h) - v^n \quad (30)$$

with

$$S_2 = -2\Omega\Delta t([(1-\alpha_1)\overline{u}^{\lambda\phi}\sin\phi]_d + \alpha_1\overline{u}^{\lambda\phi}\sin\phi) - \frac{g\Delta t}{a}([(1-\alpha_3)\delta_\phi h]_d + \alpha_3\delta_\phi h), \quad (31)$$

where the metric terms are implicit in the finding of the departure point in the semi-Lagrangian scheme.

In the full three dimensional equations the equation of state is used as the basis for forming the Helmholtz equation, whilst in the SWE the continuity equation is used. The Helmholtz equation is derived as follows.

Assume that the continuity equation holds at time level $n+1$

$$\frac{\partial h^{*\,n+1}}{\partial t} + \nabla.(\mathbf{u}h^*)^{n+1} = 0 \quad (32)$$

and define $h' = h^{n+1} - h^n$, with similar definitions for u' and v'. Equation (32) is thus

$$\frac{h'}{\Delta t} + \nabla.((\mathbf{u} + \mathbf{u}')(h^* + h')) = 0 \tag{33}$$

which when expanded and with the quadratic term in $\mathbf{u}'h'$ neglected gives

$$\frac{h'}{\Delta t} + \nabla.(h^*\mathbf{u}' + \mathbf{u}h') = -\nabla.(\mathbf{u}h^*). \tag{34}$$

To obtain the Helmholtz equation in terms of one unknown, h', we need to write $\mathbf{u}'$ in terms of h' and the variables at time level n. Equations (1) and (2) are linearised with respect to the corrections, giving

$$u' - \alpha_1\Delta t(\frac{-1}{a}\frac{\partial u}{\partial \phi} + 2\Omega \sin\phi)v' = R_1 - \alpha_3\Delta t\frac{g}{a\cos\phi}\frac{\partial h'}{\partial \lambda}, \tag{35}$$

$$\alpha_1\Delta t(\frac{\frac{\partial v}{\partial \lambda} + u\sin\phi}{a\cos\phi} + 2\Omega\sin\phi)u' + v' = R_2 - \alpha_3\Delta t\frac{g}{a}\frac{\partial h'}{\partial \phi}. \tag{36}$$

v' is eliminated from equation (35) and u' is eliminated from equation (36) giving

$$Ju' = R_1 - \alpha_3\Delta t\frac{g}{a\cos\phi}\frac{\partial h'}{\partial \lambda} + \alpha_1\Delta t(\frac{-1}{a}\frac{\partial u}{\partial \phi} + 2\Omega\sin\phi)(R_2 - \alpha_3\Delta t\frac{g}{a}\frac{\partial h'}{\partial \phi}) \tag{37}$$

$$Jv' = R_2 - \alpha_3\Delta t\frac{g}{a}\frac{\partial h'}{\partial \phi} - \alpha_1\Delta t(\frac{\frac{\partial v}{\partial \lambda} + u\sin\phi}{a\cos\phi} + 2\Omega\sin\phi)(R_1 - \alpha_3\Delta t\frac{g}{a\cos\phi}\frac{\partial h'}{\partial \lambda}) \tag{38}$$

where

$$J = 1 + \alpha_1^2\Delta t^2(\frac{-1}{a}\frac{\partial u}{\partial \phi} + 2\Omega\sin\phi)(\frac{\frac{\partial v}{\partial \lambda} + u\sin\phi}{a\cos\phi} + 2\Omega\sin\phi). \tag{39}$$

Discretising the resulting equations gives

$$u' = R_1J_u^{-1} - J_u^{-1}\alpha_3\Delta t\frac{g}{a\cos\phi}\delta_\lambda h' + F_u\left(\overline{R_2}^{\lambda\phi} - \alpha_3\Delta t\frac{g}{a}\overline{\delta_\phi h'}^{\lambda\phi}\right) \tag{40}$$

$$v' = R_2J_v^{-1} - J_v^{-1}\alpha_3\Delta t\frac{g}{a}\delta_\phi h' - F_v\left(\overline{R_1}^{\lambda\phi} - \alpha_3\Delta t\overline{\frac{g}{a\cos\phi}\delta_\lambda h'}^{\lambda\phi}\right) \tag{41}$$

$$J_u = 1 + \alpha_1^2\Delta t^2(2\Omega\sin\phi - \frac{1}{a}\delta_{2\phi}u)(2\Omega\sin\phi + \frac{\delta_\lambda\overline{v}^\phi + u\sin\phi}{a\cos\phi}) \tag{42}$$

$$J_v = 1 + \alpha_1^2\Delta t^2(2\Omega\sin\phi - \frac{1}{a}\delta_\phi\overline{u}^\lambda)(2\Omega\sin\phi + \frac{\delta_{2\lambda}v + \overline{u}^{\lambda\phi}\sin\phi}{a\cos\phi}) \tag{43}$$

where F_u and F_v are defined by

$$F_u = \alpha_1\Delta t(2\Omega\sin\phi - \frac{1}{a}\delta_{2\phi}u)J_u^{-1} \tag{44}$$

$$F_v = \alpha_1 \Delta t (2\Omega \sin\phi + \frac{\delta_{2\lambda} v + \overline{u}^{\lambda\phi} \sin\phi}{a\cos\phi}) J_v^{-1}. \tag{45}$$

Substituting the resulting equations for u' and v' in terms of h' into the discretized form of equation (34) then gives

$$\begin{aligned} h' &+ \frac{\Delta t}{a\cos\phi}\delta_\lambda(\overline{h^*}^\lambda J_u^{-1} R_1 + \overline{h^*}^\lambda F_u \overline{R_2}^{\lambda\phi} - \overline{h^*}^\lambda \alpha_3 J_u^{-1} \Delta t \frac{g}{a\cos\phi}\delta_\lambda h' - \overline{h^*}^\lambda \alpha_3 \Delta t \frac{g}{a}\overline{\delta_\phi h'}^{\lambda\phi}) \\ &+ \frac{\Delta t}{a\cos\phi}\delta_\phi[(\overline{h^*}^\phi J_v^{-1} R_2 - \overline{h^*}^\phi \overline{R_1}^{\lambda\phi} F_v - \overline{h^*}^\phi \alpha_3 J_v^{-1} \Delta t \frac{g}{a}\delta_\phi h' + \overline{h^*}^\phi \alpha_3 \Delta t \overline{\frac{g}{a\cos\phi}\delta_\lambda h'}^{\lambda\phi})\cos\phi] \\ &+ \frac{\Delta t}{a\cos\phi}\delta_\lambda(u\overline{h'}^\lambda) + \frac{\Delta t}{a\cos\phi}\delta_\phi(v\overline{h'}^\phi \cos\phi) \\ &= -\frac{\Delta t}{a\cos\phi}\delta_\lambda(u\overline{h^*}^\lambda) - \frac{\Delta t}{a\cos\phi}\delta_\phi(v\overline{h^*}^\phi \cos\phi). \end{aligned} \tag{46}$$

This is a variable coefficient Helmholtz equation of the form

$$\begin{aligned} \frac{1}{a\cos\phi}\frac{\partial}{\partial\lambda}\left(\frac{A}{a\cos\phi}\frac{\partial h'}{\partial\lambda} + A_2\overline{\frac{\partial h'}{\partial\phi}}^{\lambda\phi}\right) &+ \\ \frac{1}{a\cos\phi}\frac{\partial}{\partial\phi}\left(\frac{B\cos\phi}{a}\frac{\partial h'}{\partial\phi} - B_2\cos\phi\overline{\frac{1}{\cos\phi}\frac{\partial h'}{\partial\lambda}}^{\lambda\phi}\right) &+ \\ \frac{1}{a\cos\phi}\frac{\partial(Dh')}{\partial\lambda} + \frac{1}{a\cos\phi}\frac{\partial(Eh'\cos\phi)}{\partial\phi} - Gh' &= RHS \end{aligned} \tag{47}$$

where RHS is comprised of all the terms which do not involve h'. This equation is solved using a multigrid solver.

Now set

$$u_1 = u^n + \alpha_1 u' \tag{48}$$

$$v_1 = v^n + \alpha_1 v' \tag{49}$$

and obtain new estimates of $u^{n+1} - u^n$, $v^{n+1} - v^n$, u'', v'' respectively by solving

$$u'' = u_{1d} - u_1 + S_1 + \Delta t[2\Omega\alpha_1 \overline{v'}^{\lambda\phi} \sin\phi - \frac{g}{a}\alpha_3 \frac{\delta_\lambda h'}{\cos\phi}] \tag{50}$$

and

$$v'' = v_{1d} - v_1 + S_2 - \Delta t[2\Omega\alpha_1 \overline{u'}^{\lambda\phi} \sin\phi + \frac{g}{a}\alpha_3 \delta_\phi h'], \tag{51}$$

where the departure point of the trajectory is calculated using the wind field (u_1, v_1).

Finally set

$$u^{n+1} = u^n + u'' \tag{52}$$

$$v^{n+1} = v^n + v'' \tag{53}$$

$$h^{n+1} = h^n + h'. \tag{54}$$

Note that h could also be updated by

$$h^{n+1} = h^n - \frac{\Delta t}{a\cos\phi}\delta_\lambda(u_1\overline{h}^\lambda) - \frac{\Delta t}{a\cos\phi}\delta_\phi(v_1\overline{h}^\phi\cos\phi) \tag{55}$$

but this is not consistent with the Helmholtz equation derived above since it does not include the $\nabla.(h'\boldsymbol{u})$ term. To use this version the first derivative terms from equation (46) should be omitted, i.e. set the coefficients D and E of equation (47) to zero.

A number of different procedures were used for the calculation of the departure points, e.g. [9], and a number of different interpolation methods were tested.

4 The Test Cases

The problems investigated are all the test cases from [13]. These are presented below together with an outline of what they set out to simulate. The complete suite of test cases from [13], systematically tests areas of the advection code. The cases include an analytic problem to test the advection part of the scheme, steady state problems with analytic results, forced SWE, a problem with orography (surface topography) and finally a problem involving actual observed data. Various error measures are described in [13], and the complete range is detailed in Section 4.8 together with a guide to which error measures are employed with which test case.

4.1 Test Case 1

The first test case does not deal with the full SWE but solely with the advective part. It may be implemented in full shallow water codes by simply overwriting the calculated velocity field with the specified velocity field at all times.

This case is a test of the ability of the numerical scheme to cope with the transport of a disturbance around the globe. Different orientations of the advecting wind are specified. An initial height field is specified together with a velocity field which is analytically divergence free. The advecting wind is given by

$$u = u_0(\cos\phi\cos\alpha + \sin\phi\cos\lambda\sin\alpha), \tag{56}$$

$$v = -u_0 \sin\lambda \sin\alpha, \tag{57}$$

where the parameter α is the angle between the axis of solid body rotation and the polar axis of the spherical coordinate system.

The initial height field is a cosine bell given by

$$h(\lambda,\phi) = \begin{cases} \frac{h_0}{2}(1+\cos(\frac{\pi r}{R})) & \text{if} \quad r < R \\ 0 & \text{if} \quad r \geq R, \end{cases} \tag{58}$$

where $h_0 = 1000\text{m}$, $R = a/3$, a is the radius of the earth and r is the great circle distance between (λ,ϕ) and the centre of the cone, which is initially at $(\lambda_c,\phi_c) = (3\pi/2, 0)$, where

$$r = a\cos^{-1}[\sin\phi_c \sin\phi + \cos\phi_c \cos\phi \cos(\lambda - \lambda_c)]. \tag{59}$$

The initial height field actually used is $h + h_0$, where h is as defined in (55). This point is important as in a number of places height weighted velocity fields are used in calculations and if the height field is zero then the equations become undefined, (see [10]).

The true solution of the problem is that the cone rotates around the globe without any change in shape. It is possible to calculate the expected centre of the cone at all times, so comparisons between the true solution and the calculated solution can be made.

4.2 Test Case 2

The second test case is a steady state solution of the SWE. It consists of zonal flow with the corresponding geostrophic height field. The advecting wind is at an angle α to the equator.

The velocity fields are initially, and for all time,

$$u = u_0(\cos\phi\cos\alpha + \cos\lambda\sin\phi\sin\alpha), \tag{60}$$

$$v = -u_0 \sin\lambda \sin\alpha, \tag{61}$$

while the analytic h field is given by

$$h = h_0 - \frac{u_0}{g}(a\Omega + \frac{u_0}{2})(\sin\phi\cos\alpha - \cos\lambda\cos\phi\sin\alpha)^2. \tag{62}$$

In [13], it is suggested that it might be necessary to modify the initial wind and height field so that they satisfy a discrete geostrophic balance relationship. This discrete balance was

implemented here as was the analytic data. To satisfy discrete geostrophic balance we need, on a B-grid,

$$u = \frac{-g}{af}\overline{\delta_\lambda h}^{\phi}, \tag{63}$$

$$v = \frac{g}{af\cos\phi}\overline{\delta_\phi h}^{\lambda}, \tag{64}$$

where the coriolis term f is given by

$$f = 2\Omega(\sin\phi\cos\alpha - \cos\lambda\cos\phi\sin\alpha). \tag{65}$$

No averaging is required to satisfy geostrophic balance on a C-grid.

The parameters used in the tests described here are $u_0 = 2\pi a/(12\text{days})$ and $h_0 = 2.94\times10^4/g$ while α takes the values, $\alpha = 0.0, 0.005, \frac{\pi}{2} - 0.005, \frac{\pi}{2}$. The code is run for 5 days.

4.3 Test Case 3

This case is similar to the previous one except that the wind field is only non-zero in a limited region. The easiest way to define the wind and height fields is to start with a (λ', ϕ') coordinate system coincident with the earth's rotation axis and then rotate it by an angle α to the coordinate system(λ, ϕ). Since it is difficult to write the equations straight down in the (λ, ϕ) system the fields are defined in stages.

Let the velocity components (u', v') be given by

$$u' = u_0 b(x) b(x_e - x) e^{4/x_e}, \tag{66}$$

$$v' = 0, \tag{67}$$

where

$$b(x) = \begin{cases} 0 & \text{if } x \leq 0 \\ e^{-x^{-1}} & \text{if } 0 < x \end{cases} \tag{68}$$

and

$$x = x_e(\phi' - \phi_b)(\phi_e - \phi_b)^{-1}. \tag{69}$$

The parameters are $u_0 = 2\pi a/(12\text{days}), \phi_b = \frac{-\pi}{6}, \phi_e = \frac{\pi}{2}$, and $x_e = 0.3$.

The velocity components u and v are then defined as

$$v\cos\phi = -u'\sin\alpha\sin\lambda', \tag{70}$$

$$u\cos\lambda = v\sin\phi\sin\lambda + u'\cos\lambda', \tag{71}$$

with the coordinates related by

$$\sin\phi' = \sin\phi\cos\alpha - \cos\phi\cos\lambda\sin\alpha, \tag{72}$$

$$\sin\lambda'\cos\phi' = \sin\lambda\cos\phi. \tag{73}$$

Thus, with knowledge of λ and ϕ, equation (72) lets us determine ϕ' since $\phi' \in [-\pi/2, \pi/2]$. Using this in equation (75) we can find $\sin\lambda'$, but since $\lambda' \in [0, 2\pi]$ we need to determine which quadrant λ' falls in and this can be calculated by ensuring that

$$\cos\phi = \sin\phi'\cos\alpha + \cos\phi'\sin\alpha\cos\lambda'. \tag{74}$$

For a steady state solution h' must satisfy

$$\frac{(u')^2\tan\phi'}{a} + \frac{g}{a}\frac{\partial h'}{\partial\phi'} + fu' = 0. \tag{75}$$

The height h is difficult to find analytically, so the form in the prime system

$$h = h_0 - \frac{a}{g}\int_{-\pi/2}^{\phi'}(2\Omega\sin\tau + \frac{u'(\tau)\tan\tau}{a})u'(\tau)\delta\tau \tag{76}$$

is integrated numerically to give h. The quantity h_0 is the same as in test case 2.

The test case has been run with $\alpha = 0.0$ and $\pi/3$ for 5 days.

4.4 Test Case 4

The non-linear steady state test cases, 2 and 3, are the simplest method of measuring the adequacy of a particular numerical method. The measure of performance of a scheme on the non-linear unsteady equations is also desirable, but analytic solutions only exist in trivial cases. Thus a flow $\tilde{u}, \tilde{v}$ and $\tilde{h}$ that is similar in structure to those in the atmosphere is chosen. This flow is a solution of the forced shallow water system given below in equations (77) to (79).

The flow is a translating low pressure centre superimposed on a jet stream which is symmetrical about the equator. This field exhibits some of the properties of middle level tropospheric flow.

Test case 4 is a forced SWE problem which actually simulates the effect of a physics step in the unified model. If the forcing terms are thought of as corresponding to the correction due to the physics then, since the SWE are split into an "adjustment" step and an "advection" step, it is is possible to test whether the forcing terms should be added solely to the advection step or equally to each adjustment step.

The forced SWE are

$$\frac{du}{dt} - \left(f + \frac{u}{a}\tan\phi\right)v + \frac{g}{a\cos\phi}\frac{\partial h}{\partial\lambda} = F_u, \tag{77}$$

$$\frac{dv}{dt} + \left(f + \frac{u}{a}\tan\phi\right)u + \frac{g}{a}\frac{\partial h}{\partial\phi} = F_v, \tag{78}$$

$$\frac{dh}{dt} + \frac{h}{a\cos\phi}\left(\frac{\partial u}{\partial\lambda} + \frac{\partial v\cos\phi}{\partial\phi}\right) = F_h, \tag{79}$$

where the height of the mountains, h_s, is defined as zero and the substantive derivative is

$$\frac{d}{dt} = \frac{\partial}{\partial t} + \frac{u}{a\cos\phi}\frac{\partial}{\partial\lambda} + \frac{v}{a}\frac{\partial}{\partial\phi}. \tag{80}$$

The forcing terms in equations (77) to (79) are defined as

$$F_u = \frac{d\tilde{u}}{dt} - \left(f + \frac{\tilde{u}}{a}\tan\phi\right)\tilde{v} + \frac{g}{a\cos\phi}\frac{\partial\tilde{h}}{\partial\lambda}, \tag{81}$$

$$F_v = \frac{d\tilde{v}}{dt} + \left(f + \frac{\tilde{u}}{a}\tan\phi\right)\tilde{u} + \frac{g}{a}\frac{\partial\tilde{h}}{\partial\phi}, \tag{82}$$

$$F_h = \frac{d\tilde{h}}{dt} + \frac{\tilde{h}}{a\cos\phi}\left(\frac{\partial\tilde{u}}{\partial\lambda} + \frac{\partial\tilde{v}\cos\phi}{\partial\phi}\right). \tag{83}$$

The flow fields are given by

$$\tilde{u} = \bar{u} - \frac{\bar{\psi}_\phi}{a}, \tag{84}$$

$$\tilde{v} = \frac{\bar{\psi}_\lambda}{a\cos\phi}, \tag{85}$$

$$g\tilde{h} = g\bar{h} + f\bar{\psi}, \tag{86}$$

where

$$\bar{u} = u_0\sin^{14}(2\phi), \tag{87}$$

$$g\bar{h} = gh_0 - \int_{-\pi/2}^{\phi}[af(\tau) + \bar{u}(\tau)\tan\tau]\bar{u}(\tau)\partial\tau \tag{88}$$

and

$$\bar{\psi}(\lambda,\phi,t) = \psi_0 e^{-\sigma((1-C)/(1+C))} \tag{89}$$

with $\psi_0 = -0.03(gh_0/f_0), \sigma = (12.74244)^2, gh_0 = 10^5, f_0 = 2\Omega\sin(\pi/4)$, and

$$C = \sin\phi_0\sin\phi + \cos\phi_0\cos\phi\cos\left(\lambda - \frac{u_0}{a}t - \lambda_0\right). \tag{90}$$

The centre of the low is initially located at $(\lambda_0, \phi_0) = (0, \pi/4)$.

Results for this problem are not available due to implementation difficulties, with the compilers available being unable to evaluate the recursive functions needed to calculate all the terms in equations (84) to (90).

4.5 Test Case 5

This test case consists of zonal flow, as in test case 2, impinging on a mountain. The wind and height field are as in case 2 with $\alpha = 0$ but with $h_0 = 5960$ and $u_0 = 20$. The mountain height is given by

$$h_s = h_{s0}(1 - r/R), \tag{91}$$

where $h_{s0} = 2000, R = r/9$ and $r^2 = \min[R^2, (\lambda - \lambda_c)^2 + (\phi - \phi_c)^2]$. The centre is taken as $\lambda_c = 3\pi/2$ and $\phi_c = \pi/6$.

This tests the code when there is surface topography involved in the problem. In this case the surface is a steeply sloping mountain. The code should be run for 15 days.

4.6 Test Case 6

Rossby-Haurwitz waves are analytic solutions of the nonlinear barotropic vorticity equation on the sphere. Although they are not analytic solutions of the SWE they have been used for so long that they are now *de-facto* standard test cases.

Test case 6 is the Rossby-Haurwitz wave with R=4.

This test case has a height field that moves from east to west with no change in shape, with an angular velocity v given by

$$v = \frac{R(R+3)\omega - 2\Omega}{(1+R)(2+R)}. \tag{92}$$

The velocity components are given by

$$u = a\omega\cos\phi + aK\cos^{R-1}\phi(R\sin^2\phi - \cos^2\phi)\cos R\lambda, \tag{93}$$

$$v = -aKR\cos^{R-1}\phi\sin\phi\sin R\lambda, \tag{94}$$

and the height is obtained from the stream function by solving the balance equation, so the initial tendency of the divergence is zero:

$$gh = gh_0 + a^2A(\phi) + a^2B(\phi)\cos R\lambda + a^2C(\phi)\cos 2R\lambda, \tag{95}$$

$$A(\phi) = \frac{\omega}{2}(2\Omega + \omega)\cos^2\phi + \frac{1}{4}K^2\cos^{2R}\phi[(R+1)\cos^2\phi + (2R^2 - R - 2) - 2R^2\cos^{-2}\phi], \tag{96}$$

$$B(\phi) = \frac{2(\Omega+\omega)K}{(R+1)(R+2)}\cos^R\phi[(R^2 + 2R + 2) - (R+1)^2\cos^2\phi], \tag{97}$$

$$C(\phi) = \frac{1}{4}K^2\cos^{2R}\phi[(R+1)\cos^2\phi - (R+2)]. \tag{98}$$

The parameters are $\omega = K = 7.848 \times 10^{-6}$ and $h_0 = 8 \times 10^3$ and the code is run for 14 days.

4.7 Test Case 7

This test case is comprised of 3 sets of initial data taken from physically observed data. The observations were made at the following times:-

a) 0000 GMT December 21, 1978

b) 0000 GMT January 16, 1979

c) 0000 GMT January 9, 1979.

2D contour plots for the initial height fields were shown in [11]. These data sets test the code on a very unsymmetric problem.

The first data set, test case 7a, has strong flow over the North pole and has pointed out deficiencies in schemes which have been applied to it by previous researchers. The second data set, test case 7b, is characterised by two cutoff lows. The flow pattern develops into a typical blocking situation. The third data set, test case 7c, initially has strong zonal flow. All three cases are run for 5 days.

4.8 Error Measures

Graphical output, in the form of contour plots, of the height field and the error therein at the end of the specified run time is required for most of the test cases.

All the other measures are to be plotted against time. These other measures fall into two categories, "norms" and "invariants". The norms are normalised global errors with respect to the "true" solution. The invariants are quantities which should preferably be conserved.

Define I to be a discrete approximation to the global integral

$$I(x) = \int_0^{2\pi} \int_{-\pi/2}^{\pi/2} x(\lambda, \phi) \cos\phi d\phi d\lambda. \tag{99}$$

and let x_T be the true value of x at a time, t, and x_o be the initial value of x.

The norms to be calculated are

$$l_1(h) = \frac{I[|h(\lambda,\phi) - h_T(\lambda,\phi)|]}{I[|h_T(\lambda,\phi)|]} \tag{100}$$

$$l_2(h) = \frac{\{I[(h(\lambda,\phi) - h_T(\lambda,\phi))^2]\}^{1/2}}{\{I[h_T(\lambda,\phi)^2]\}^{1/2}} \tag{101}$$

$$l_\infty(h) = \frac{\max_{\text{all}\lambda,\phi}|h(\lambda,\phi) - h_T(\lambda,\phi)|}{\max_{\text{all}\lambda,\phi}|h_T(\lambda,\phi)|} \tag{102}$$

$$l_1(\boldsymbol{v}) = \frac{[I[\{(u(\lambda,\phi) - u_T(\lambda,\phi))^2 + (v(\lambda,\phi) - v_T(\lambda,\phi))^2\}^{1/2}]]}{I[\{u_T(\lambda,\phi)^2 + v_T(\lambda,\phi)^2\}^{1/2}]} \tag{103}$$

$$l_2(\boldsymbol{v}) = \frac{[\{I[(u(\lambda,\phi) - u_T(\lambda,\phi))^2 + (v(\lambda,\phi) - v_T(\lambda,\phi))^2]\}^{1/2}]}{\{I[u_T(\lambda,\phi)^2 + v_T(\lambda,\phi)^2]\}^{1/2}} \tag{104}$$

$$l_\infty(\boldsymbol{v}) = \frac{[\max_{\text{all}\lambda,\phi}[\{(u(\lambda,\phi) - u_T(\lambda,\phi))^2 + (v(\lambda,\phi) - v_T(\lambda,\phi))^2\}^{1/2}]]}{\max_{\text{all}\lambda,\phi}[\{u_T(\lambda,\phi)^2 + v_T(\lambda,\phi)^2\}^{1/2}]} \tag{105}$$

The normalised integral is defined as

$$I_i(\xi(t)) = \frac{I[\xi(\lambda,\phi,t)] - I[\xi(\lambda,\phi,0)]}{I[\xi(\lambda,\phi,0)]} \tag{106}$$

The following invariants are presented :-

- mass (i=1)

$$\xi = h^* \tag{107}$$

- total energy (i=2)

$$\xi = \frac{1}{2}h^*\boldsymbol{v}.\boldsymbol{v} + \frac{1}{2}g(h^2 - h_s^2) \tag{108}$$

- potential enstrophy (i=3)

$$\xi = 0.5(\zeta + f)^2/h^* \tag{109}$$

The unnormalised integrals of vorticity and divergence will also be presented since their initial values are zero.

- vorticity (i=4)

$$\xi = \zeta \tag{110}$$

- divergence (i=5)

$$\xi = \delta \tag{111}$$

The norms are calculated every time step for test cases 2 to 4 and daily for test cases 5 to 7. The invariants should be calculated for test cases 5 to 7 at every time step. Test case 1 requires only the calculation of the norms of the h field, but requires the calculation of normalized mean, variance, minimum and maximum at every time step. These are calculated as below. If

$$\overline{h} = I[h(\lambda, \phi)] \tag{112}$$

denotes the mean, the normalised mean and variance are written

$$M = \overline{h} - \overline{h_T})/\overline{h_o} \tag{113}$$

$$V = \{I[(h - \overline{h})^2] - I[(h_T - \overline{h_T})^2]\}/I[(h_o - \overline{h_o})^2] \tag{114}$$

and the maximum and minimum are

$$h_{\max} = (\max_{\text{all}\lambda,\phi} h(\lambda, \phi) - \max_{\text{all}\lambda,\phi} h_T(\lambda, \phi))/\Delta h \tag{115}$$

$$h_{\min} = (\min_{\text{all}\lambda,\phi} h(\lambda, \phi) - \min_{\text{all}\lambda,\phi} h_T(\lambda, \phi))/\Delta h \tag{116}$$

where Δh is the difference between the maximum and minimum values of the true solution initially.

5 Results and Comparisons

In this section the graphical and numerical results are presented.

The results for test case 1 have been produced in [10] and the conclusions are reiterated here.

The TVD schemes reduce the oscillations, as expected, but with a resultant loss in the height field. The superbee limiter produced a reduction to about 75% while the van Leer limiter produced a reduction to about 50% of the original maximum height.

For equatorial flow the best results were produced by the Heun scheme together with filtering and diffusion. The filtering reduced the numerical oscillations in the polar regions while the diffusion reduced the numerical oscillations behind the cone. Thus while the actual contours are slightly more spread out the loss in height is not as severe.

A semi-Lagrangian code [1] has also been implemented, on a C-grid rather than a B-grid, and while it compares well for all advecting wind directions the best result is that for cross polar flow [10].

Results produced by the NCAR STSWM model [5] are used in problems 5-7 as "reference solutions". These were retrieved by using the netcdf files provided by NCAR of their test runs. For a full comparison [6] shows a full set of results as does [7].

A large number of test runs were carried out and a comparison of a number of different solution strategies were made.

The full results for the Eulerian schemes have already been presented in [11].

Indeed, the results reproduced here will be those of the semi-Lagrangian scheme, and these show that the scheme produces favourable results.

It should be noted that the Heun scheme code only worked for timesteps of 10 minutes or less even for a 96x73 resolution grid.

The semi-Lagrangian scheme code works for a time step of up to 2 hours although above 1 hour the results start to degrade. This has led to a slight modification of the scheme where equations (48) to (53) are ignored, i.e. no second advection step is carried out and u and v are updated using

$$u^{n+1} = u^n + u' \tag{117}$$

$$v^{n+1} = v^n + v' \tag{118}$$

This has led to the use of a 6 hour timestep without degredation of the results. This revised scheme is that currently used in the 3-D test schemes.

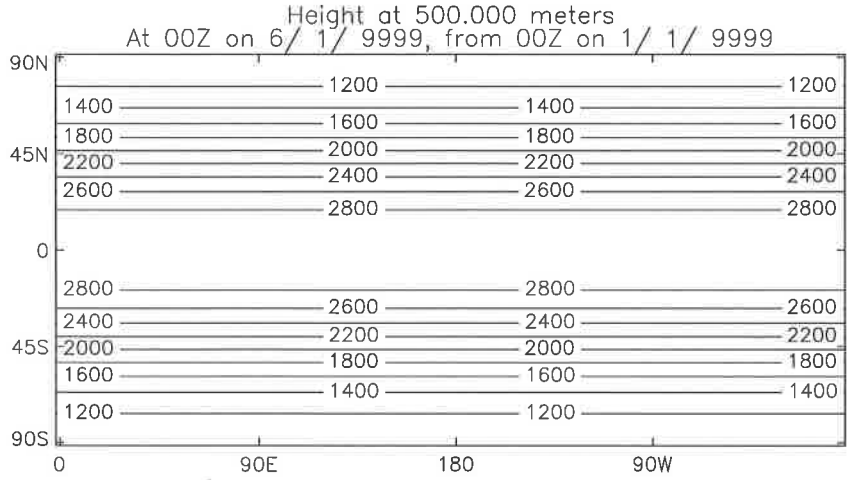

Figure 2: Solution of test case 2.

Test case 2 is the steady-state solution and the code works perfectly on this case as can be seen in Figure 2. The initial data and the solution are almost identical (the maximum difference in h is 0.4).

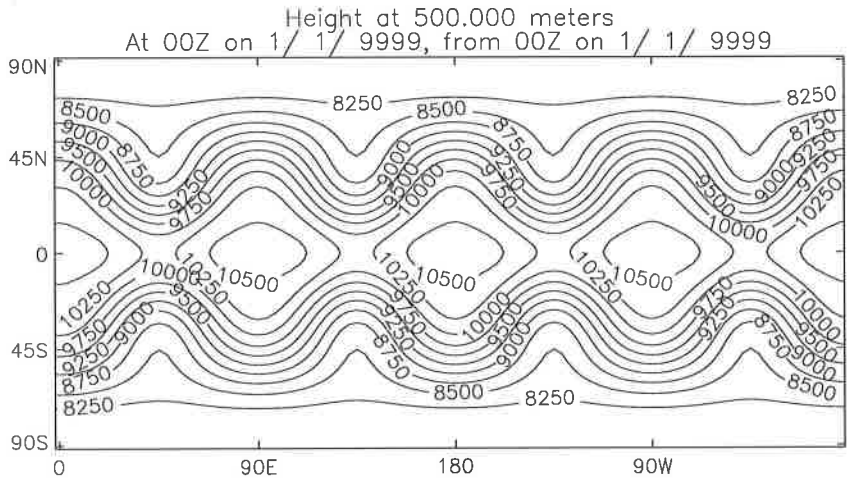

Figure 3: Test case 6, initial data.

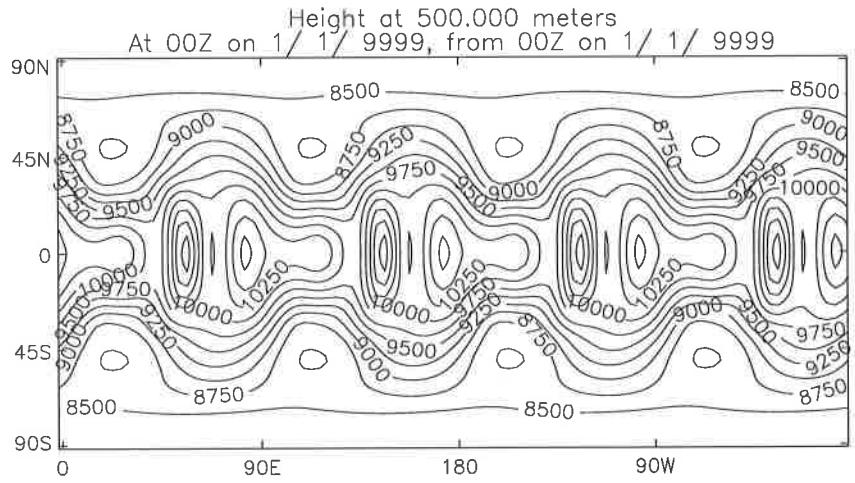

Figure 4: Test case 6, Heun solution, 10 minute time step.

Figure 3 shows the initial data for test case 6, the Rossby-Haurwitz wave number 4 problem. Figure 4 shows the result of using the Heun scheme with a 10 minute time step. It can be seen that it is starting to look as each wave is splitting into two components.

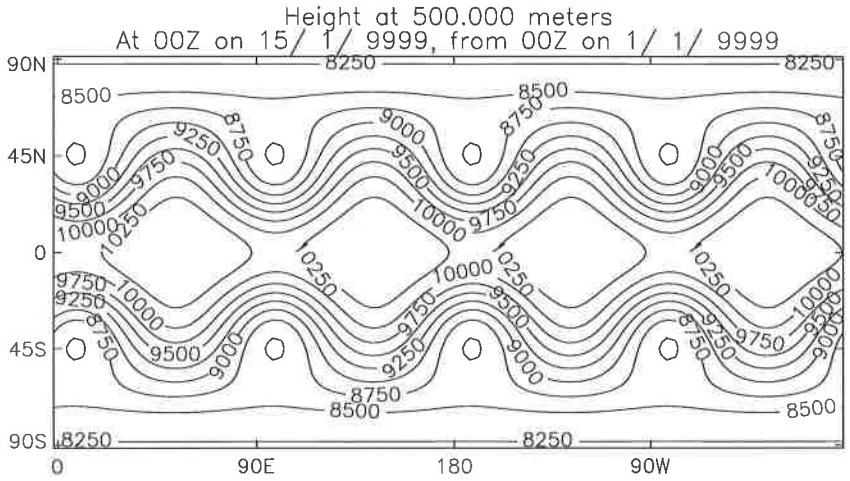

Figure 5: Test case 6, semi-Lagrangian solution, 10 minute time step.

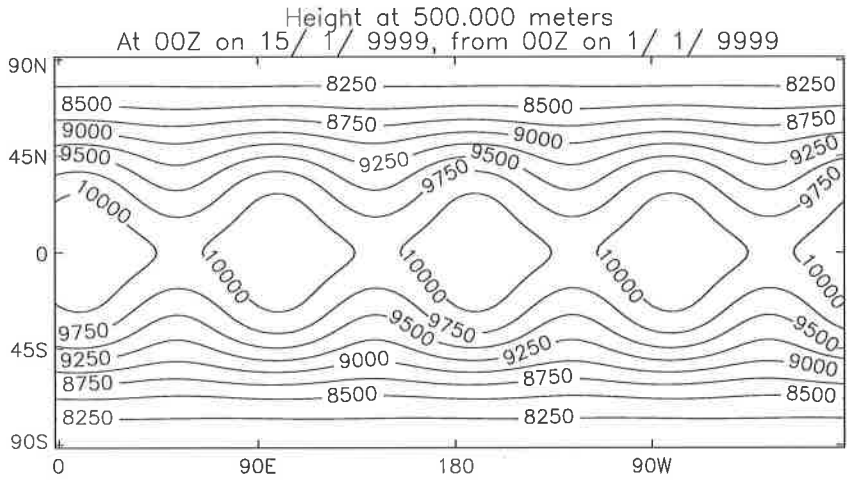

Figure 6: Test case 6, revised semi-Lagrangian solution, 6 hour time step.

Figure 5 shows that for a 10 minute time step the semi-Lagrangian scheme produces results which compare favourably with the Heun scheme and figure 6 shows that if the revised scheme is used then even with a 6 hour time step the result is still sasisfactory. The numerical errors for the Heun scheme result and for the 6 hour time step revised step are very similar, while the semi-Lagrangian 10 minute time step is better than both.

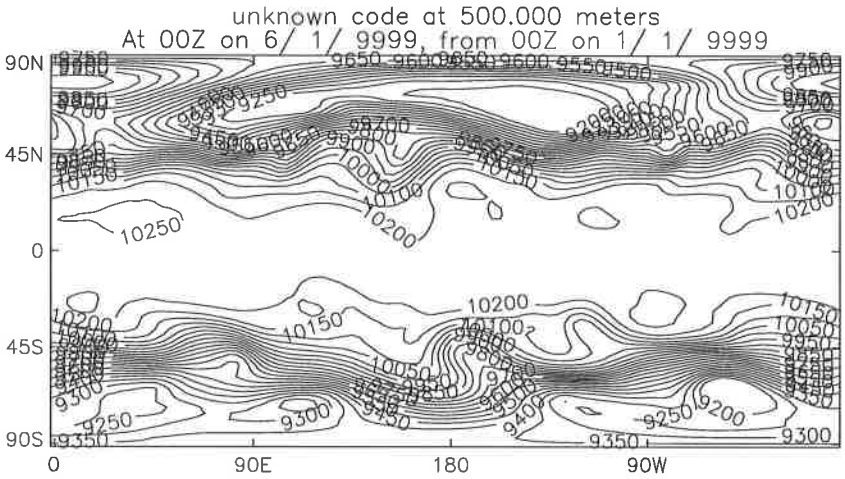

Figure 7: Reference solution of test case 7a.

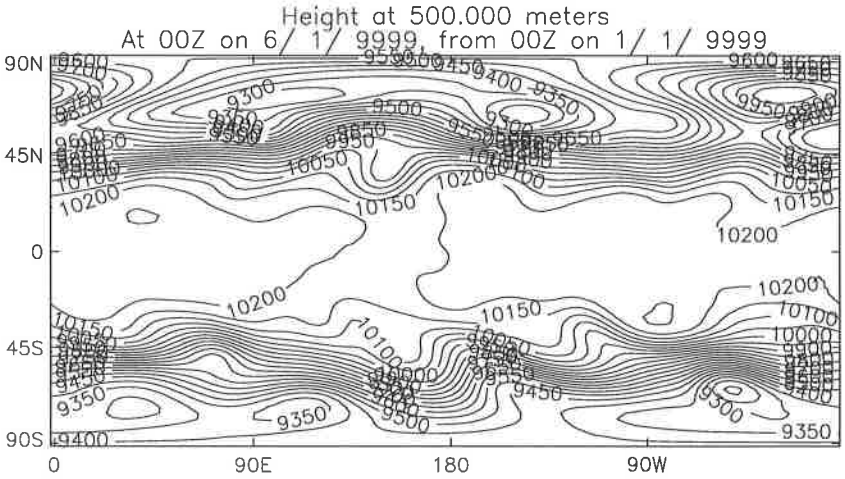

Figure 8: Solution of test case 7a, 3 hour time step.

Figure 7 shows the reference solution for test case 7a while figure 8 shows the result for the semi-Lagrangian scheme with a 3 hour time step.

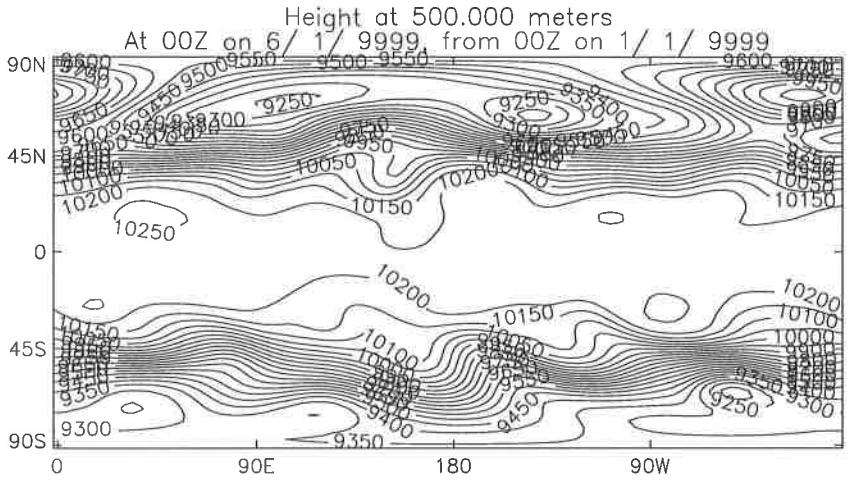

Figure 9: Solution of test case 7a, 30 min time step.

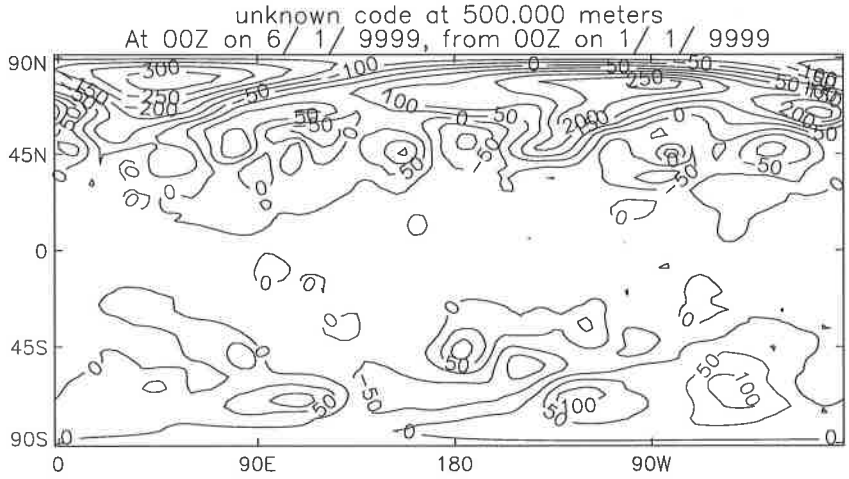

Figure 10: Error in solution of test case 7a, 30 minute time step.

Figure 9 shows the result produced by the semi-Lagrangian scheme with a 30 minute time step. This is almost identical to the result for the same scheme with a 10 minute time step. Figure 10 shows the error field from the same run. The errors near the north pole are caused by the introduction of rounding error when calculating the departure points for the trajectories near the poles.

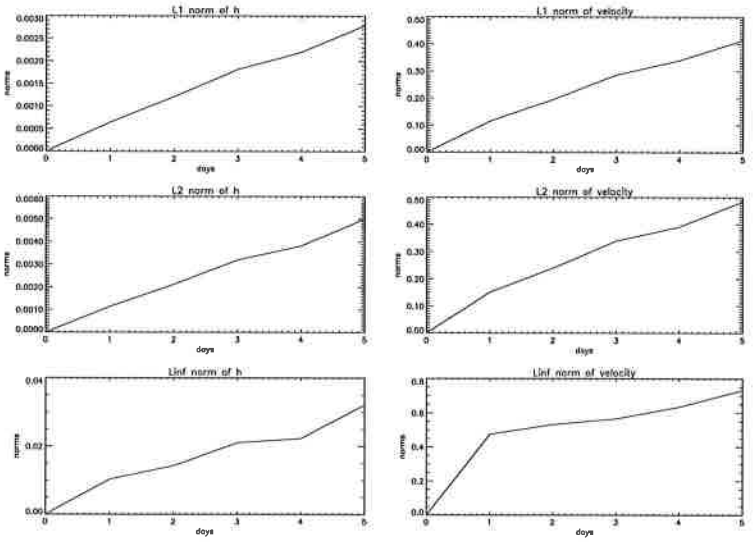

Figure 11: Norms relating to test case 7a, 30 minute time step.

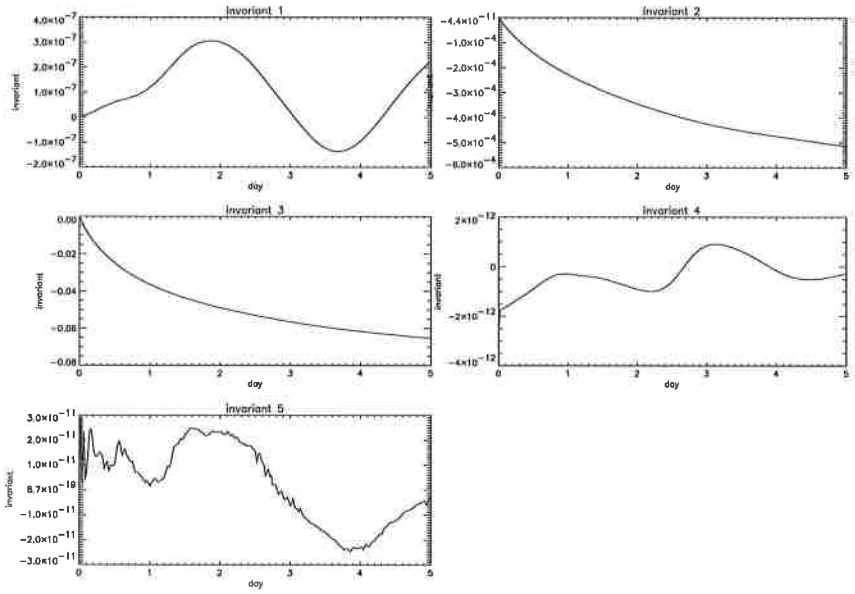

Figure 12: Invariants relating to test case 7a, 30 minute time step.

Figure 11 shows graphs of the error norms for the semi-Lagrangian scheme with a 30 minute time step. The error norms are only calculated at one day intervals. Figure 12 shows graphs of the invariants for the same run. Noting the values on the y-axes of the graphs, the only invariants which do not stay very close to zero are the total energy (graph 2) and the potential enstrophy (graph 3). The rest are very well preserved.

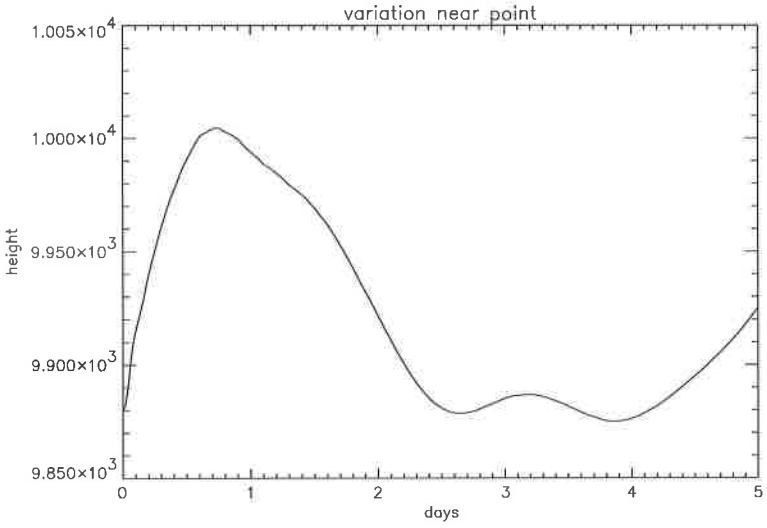

Figure 13: Height values near a point, test case 7a.

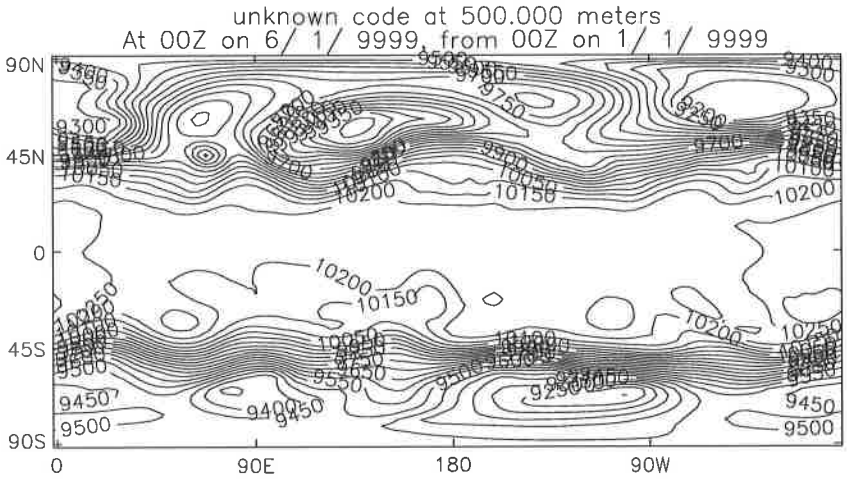

Figure 14: Reference solution of test case 7b.

Figure 13 shows the variation of height at a point over the complete run of the semi-Lagrangian scheme with a 30 minute time step.

Figure 14 shows the reference solution for test case 7b.

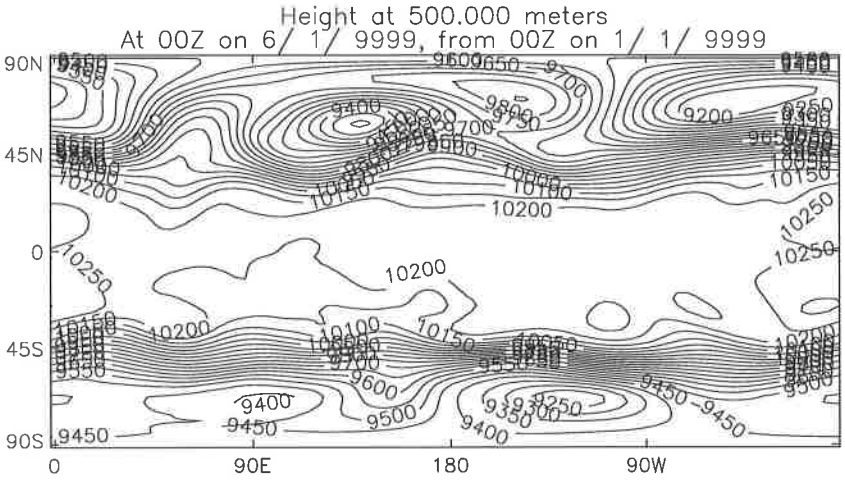

Figure 15: Solution of test case 7b, 30 minute time step.

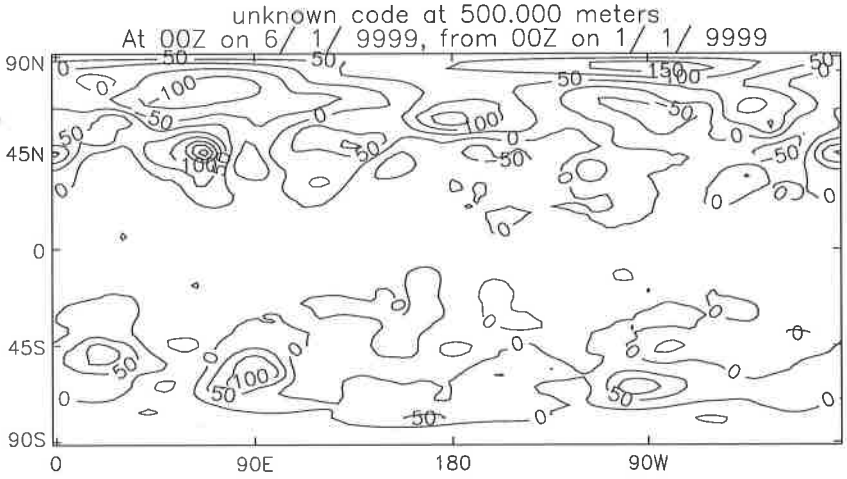

Figure 16: Errors in solution of test case 7b.

Figure 15 shows the result for the semi-Lagrangian scheme with a 30 minute time step. Figure 16 shows the error field for the solution shown in figure 15. Since the flow is not as strongly cross polar as test case 7a the errors are smaller in magnitude.

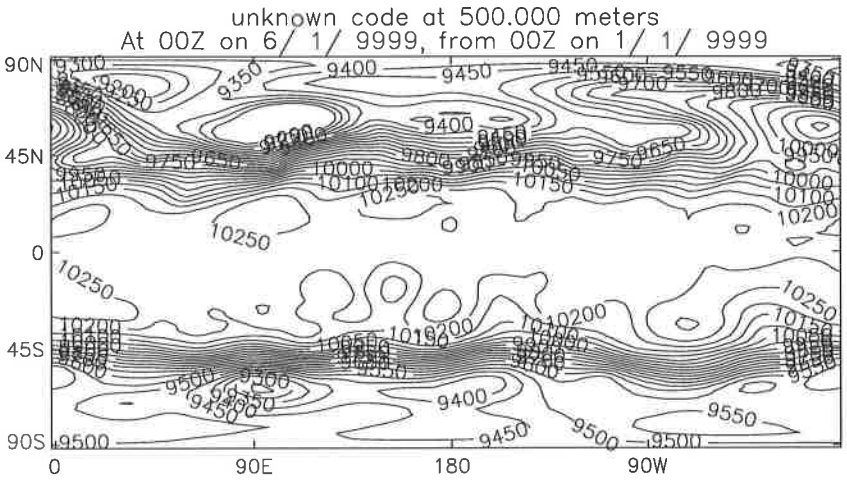

Figure 17: Reference solution of test case 7c.

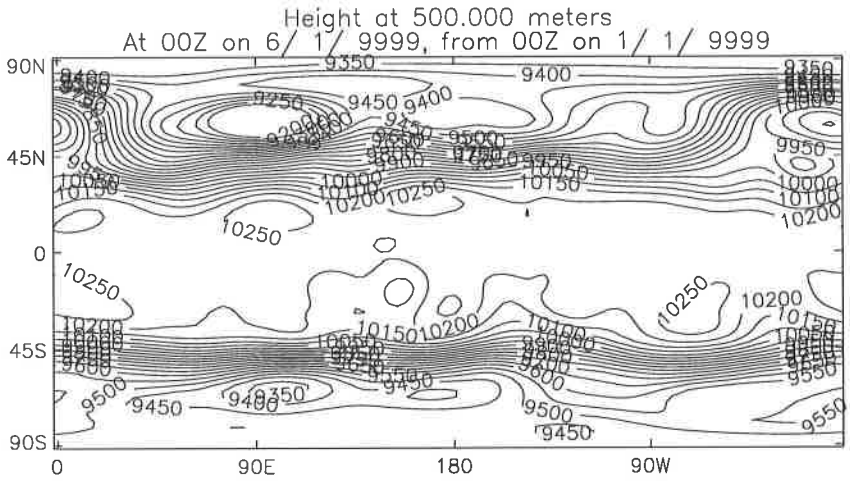

Figure 18: Solution of test case 7c, 30 minute time step.

Figure 17 shows the reference solution for test case 7c while figure 18 shows the solution for the semi-Lagrangian scheme with a 30 minute time step.

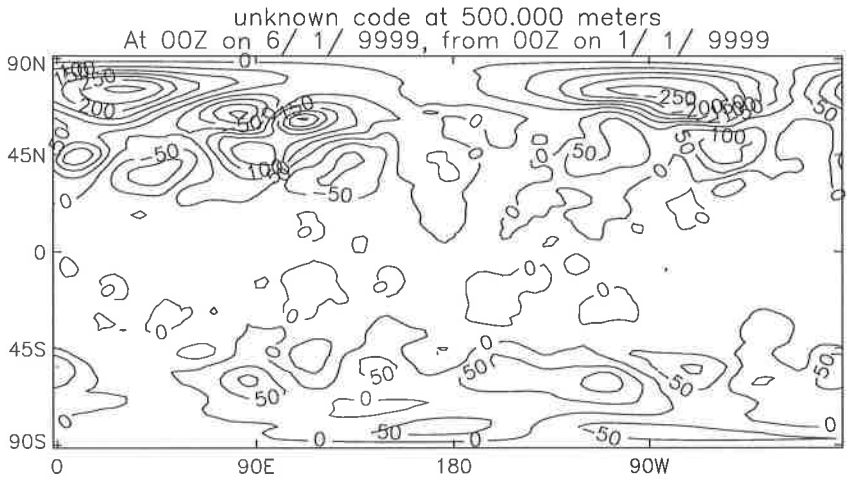

Figure 19: Error in solution of test case 7c.

Figure 19 shows the error field for the solution shown in figure 18. Again the errors near the pole are caused by the introduction of rounding errors in the calculation of the trajectories over the poles.

6 Conclusions

The Eulerian schemes and the semi-Lagrangian scheme have been compared on the test set described in [13]. The results reported in [10] show that on the pure advection test case, of the Eulerian schemes tested, the currently employed Heun scheme was the best. When the semi-Lagrangian scheme was used on the same test case it improved results for cross polar flows while being only slightly worse for equatorial flows.

The results of running the codes on the other test cases show that the semi-Lagrangian scheme produces improvements in the L_2 error of approximately 10%. The main advantage of the semi-Lagrangian scheme is that it works with a much longer timestep, e.g. 6 hours, as opposed to the the Heun scheme which only operated with a 10 minute time step. This shows that the semi-implicit semi-Lagrangian scheme is worth investigating as a successor for the current split-explicit Eulerian based Heun scheme.

Acknowledgements

I would like to thank the Meteorological Office for the funding of the contract from which this report was produced and Dr Mike Cullen, Dr Terry Davies and Dr Mark Mawson for their advice and helpful suggestions. I also wish to thank Mark for providing the original semi-Lagrangian and multigrid subroutines. I would also like to thank Dr Mike Baines and Dr Peter Sweby for useful discussions during the course of this work.

References

[1] **J.R. Bates, F.H.M. Semazzi, R.W. Higgins and S.R.M. Barros**, (1990), *Integration of the Shallow Water Equations on the Sphere using a Vector Semi-Lagrangian Scheme with a Multigrid Solver*, Mon. Wea. Rev. **118**, pp 1615-1627

[2] **M.J.P. Cullen and T. Davies**, (1991), *A Conservative Split-Explicit Integration Scheme with Fourth-Order Horizontal Advection*, J. R. Meteorol. Soc.**117**, pp 993-1002

[3] **M.J.P. Cullen, T. Davies and M.H. Mawson**, (1993), *Conservative Finite Difference Schemes for a Unified Forecast/Climate Model*, Met. Office Unified Model Documentation Paper No. 10, Version No. 24

[4] **M.J.P. Cullen, T. Davies and M.H. Mawson**, (1994), *A Semi Implicit Integration Scheme for the Unified Model*, Met. Office Forecasting Research Working Paper No. 154

[5] **J.J. Hack and R. Jakob**, (1992), *Description of a Global Shallow Water Model Based on the Spectral Transform Method.*, NCAR Technical Note, NCAR/TN-343+STR

[6] **Ross P. Heikes and David A. Randall**, (1993) *The Shallow Water Equations on a Spherical Geodesic Grid*, Colorado State University, Dept. Atm. Sci Paper, 524

[7] **R. Jakob, J.J. Hack and D.L. Williamson**, (1993), *Solutions to the Shallow Water Test Set Using the Spectral Transform Method*, NCAR Technical Note, NCAR/TN-388-STR

[8] **S.A. Leathwood and M.J.P. Cullen**, (1990), *A Positive Definite Advection Scheme Suitable for the Unified Model*, Met. Office Short-Range Forecasting Research Technical Note No. **55**

[9] **J.L. McGregor**, (1993), *Economical Determination of Departure Points for Semi-Lagrangian Models*, Mon. Wea. Rev **121**, pp 221-230

[10] **A.J. Malcolm**, (1994), *Testing Advection Schemes for the Shallow Water Equations on a Set of Test Problems, I*, Met. Office Forecasting Research Technical Note No. 83

[11] **A.J. Malcolm**, (1994), *Evaluation of a Numerical Scheme on a Set of Test Problems for the Shallow Water Equations*, Met. Office Forecasting Research Technical Report No. 122

[12] **B.L. Marshall**, (1989), *Tests of the New Heun Advection Scheme*, Met. Office 11 Technical Note No. **31**

[13] **D.L. Williamson, J.B. Drake, J.J. Hack, R. Jakob and P.N. Swarztrauber**, (1992), *A Standard Test Set for Numerical Approximations to the Shallow Water Equations in Spherical Geometry*, J. Comp. Phys. **102**, pp 211-224